IEEE Photonics Journal
An IEEE Photonics Society Publication

Temperature Dependence of the Steering Angles of a Silicon Photonic Optical Phased Array

Volume 12, Number 2, April 2020

Pedro Andrei Krochin Yepez
Ulrike Scholz
Andre Zimmermann

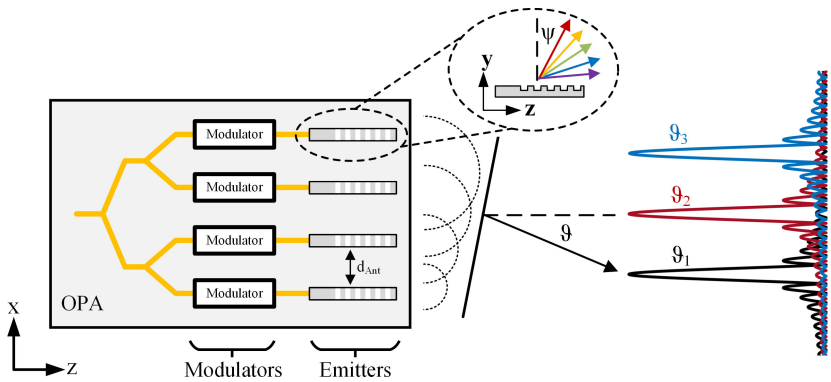

DOI: 10.1109/JPHOT.2020.2966618

Temperature Dependence of the Steering Angles of a Silicon Photonic Optical Phased Array

Pedro Andrei Krochin Yepez,[1,2] **Ulrike Scholz**,[1] **and Andre Zimmermann** [2,3]

[1]Department of Microsystems and Nanotechnologies (CR/ARY), Corporate Sector Research and Advance Engineering, Robert Bosch GmbH, Renningen 71272, Germany
[2]Institute for Micro Integration (IFM), University of Stuttgart, Stuttgart 70569, Germany
[3]Hahn-Schickard, Stuttgart 70569, Germany

DOI:10.1109/JPHOT.2020.2966618

Manuscript received November 26, 2019; accepted January 10, 2020. Date of publication January 13, 2020; date of current version March 9, 2020. Corresponding author: Pedro Andrei Krochin Yepez (e-mail: akrochin@hotmail.com).

Abstract: Silicon photonic optical phased arrays leveraging from the well established CMOS fabrication process have become promising candidates to realize miniaturized beam steering systems. While different implementations of optical phased arrays have been successfully demonstrated, no investigations on the influence of thermal distortions on the response of these systems have been performed so far. Due to the high thermo-optic coefficient of silicon, the refractive index and thus the functionality of silicon photonic components depend strongly on the temperature. In highly integrated systems, consisting of several photonic components, in which laser sources and control electronics are directly integrated on top of the photonic IC, heat dissipated by active components leads to temperature gradients and offsets, affecting the functionality of the photonic system. Optical phased arrays consisting of an array of phase sensitive components, are particularly sensitive towards temperature. Therefore, precise investigations of the temperature dependence of the OPA functionality are required. This article aims to expand the understanding of the influence of thermal distortions on the steering angles of optical phased arrays. Thereto, analytical expressions describing the temperature dependence of the steering angles are provided and experimentally validated. The expressions are provided in a general form so that they can be applied to any OPA system regardless of its implementation.

Index Terms: Photonic integrated circuits (PIC), silicon photonics, optical phased arrays (OPAs).

1. Introduction

Optical beam steering is required for applications ranging from sensing and imaging to free space optical communications [1]–[3]. State-of-the-art beam steering systems rely on mechanical components, which in addition to being slow and bulky, bring along reliability concerns [4]–[7]. To reduce the system dimensions, to increase the scanning speed as well as to reduce reliability issues, solid-state optical beam steering systems are desired [8], [9]. Optical phased arrays (OPAs) consisting of an array of optical emitters, allow for non-mechanical beam steering, by controlling the relative phase difference between neighboring emitters. Furthermore, due to their compatibility with the well established CMOS fabrication processes, a large number of silicon photonic OPAs can

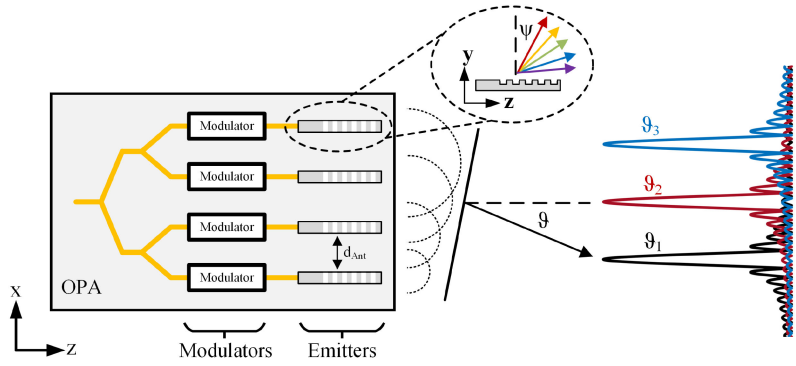

Fig. 1. Schematic representation of a four channels optical phased array consisting of optical modulators and grating antennas as optical emitters. The optical modulators are used to change the relative phase ($\Delta\varphi$) between neighboring channels allowing for beam steering in the ϑ direction. The grating antennas are used for two dimensional beam steering. By tuning the wavelength of the laser source, the emission angle ψ is modified.

be fabricated at extremely low costs, making them promising candidates to become the successors of current mechanical beam steering systems. As shown in Figure 1, two dimensional optical beam steering can be achieved using an optical phased array consisting of N optical modulators placed behind grating antennas. Using the optical modulators behind the antennas, the relative phase difference $\Delta\varphi$ between neighboring antennas is changed, allowing to modify the angle ϑ at which light is emitted. The phase controlled steering angle ϑ is defined by:

$$\sin(\vartheta) = \frac{\lambda}{2\pi \cdot d_{\text{Ant}}} \cdot \Delta\varphi, \tag{1}$$

where λ stands for the emission wavelength of the laser source and d_{Ant} for the distance between neighboring emitters in the array.

Two dimensional beam steering is achieved by employing grating structures as optical antennas [10]–[12]. Since the emission angle ψ of the gratings antennas depends on the wavelength λ, beam steering is easily achieved using tunable laser sources. The wavelength controlled angle ψ is defined by:

$$\sin(\psi) = \frac{n_{\text{eff}} - \frac{\lambda}{\Lambda}}{n_{\text{clad}}}, \tag{2}$$

where n_{eff} stands for the effective refractive index of the antennas, n_{clad} for the refractive index of the cladding covering the antennas, and Λ for the period of the grating.

The beam divergence as well as the field-of-view achieved by an optical phased array depends on the number of channels N as well as on the distance d_{Ant} between the optical antennas. Therefore, to improve the performance of OPAs, it is desired to increase the number of antennas, while simultaneously reducing their pitch (d_{Ant}) [13]. However, to avoid light coupling between neighboring antennas, the pitch must be similar or larger than the wavelength of light [14]. A detailed description of the relation between the different OPA parameters and the OPA performance is out of the scope of this work and for further information the reader is referred to other literature [15]–[17]. While different implementations of optical phased arrays with different parameters (N and d_{Ant}) as well as using different types of optical modulators have already been successfully demonstrated [18], to the best of our knowledge, no investigations regarding the influence of thermal distortions on the performance of these systems have been done so far.

Thermal management of such highly integrated, phase sensitive systems is one major challenge hindering their commercialization. On the one hand, due to the direct relation between the refractive index n and the optical phase φ, and owed to the large thermo-optic coefficient (TOC) of silicon

($\partial n_{Si}/\partial T \approx 1.84 \cdot 10^{-4} 1/K$ [19]), phased sensitive silicon photonic components are extremly sensitive to temperature [20]. On the other hand, the emission wavelength of semiconductor lasers also depends on the temperature. Therefore, thermal management of optical phased arrays requires not only precise understanding of the influence of undesired temperature effects on the response of the optical phased array but also appropriate measures to reduce the influence of these distortions.

Several groups have put a lot of effort in improving the performance of OPAs [21], [22], however, so-far little attention has been paid to understanding the influence of the thermal distortions on the OPA response. In this publication, the influence of two kinds of thermal distortions, namely temperature offsets and temperature gradients, on the steering angles ϑ and ψ of silicon photonic optical phased arrays is investigated. For this, analytical expressions describing the dependence of the steering angles on the temperature are derived and validated. To the best of our knowledge, this is the first time that the influence of thermal distortions on the response of optical phased arrays is investigated. In Section 2, the theoretical background required for the subsequent investigations is presented and the analytical expressions relating the steering angles to the temperature are presented. In Section 3, the experimental setup as well as the methods used for experimental validation are presented. The experimental results are presented in Section 4. Finally, in Section 5, the conclusions of this analysis are drawn.

2. Influence of Thermal Distortions on the Beam Steering Angles

2.1 Theory and Working Principle

While in most OPA systems demonstrated so far thermal distortions did not play a major role, in systems such as [23], [24], in which laser sources are directly integrated on the photonic IC or systems such as [25], [26], where the control electronics are integrated on top of the OPA, thermal distortions have a strong influence on the system response. To analyze the influence of these thermal distortions on the response of an optical phased array, two types of distortions are considered: temperature offsets and temperature gradients. Temperature offsets originate due to an inefficient heat dissipation as well as due to ambient temperature fluctuations. Temperature gradients on the other hand arise due to heat generated by laser sources and driver electronics, integrated on top of the silicon photonic IC.

As mentioned before, due to the large thermo-optic coefficient of silicon $\partial n_{Si}/\partial T$, its refractive index n is strongly dependent on the temperature T. The change of the refractive index due to temperature is given by:

$$\Delta n = n(T) - n(T_{ref}) = \frac{\partial n}{\partial T} \cdot (T - T_{ref}), \tag{3}$$

where $n(T_{ref})$ stands for the refractive index at the reference temperature T_{ref}.

The accumulated optical phase is defined as $\varphi = \frac{2\pi}{\lambda} \cdot \mathrm{OPL}$, where OPL stands for the optical path length, defined as the product between the refractive index n and the length L of the waveguide. Therefore, changing the optical path length changes the accumulated phase at the end of the waveguide. In photonic integrated circuits, the optical phase is modified by modifying the refractive index of the waveguide, so that:

$$\Delta\varphi = \frac{2\pi}{\lambda} \cdot \int_0^L \Delta n(z) \mathrm{d}z \tag{4}$$

Replacing Equation (3) into Equation (4), the relation between the optical phase shift $\Delta\varphi$ and the temperature change $\Delta T = T - T_{ref}$ is found:

$$\Delta\varphi = \frac{2\pi}{\lambda} \cdot L \cdot \frac{\partial n}{\partial T} \cdot (T - T_{ref}) \tag{5}$$

Since ϑ depends directly on the relative phase difference $\Delta\varphi$, it is evident, why it is affected by temperature. However, in addition to the optical phase, other quantities defining the emission angles in Equations (1) and (2) also depend on the temperature. The most evident temperature

dependence missing is the temperature dependence of the cladding refractive index n_{clad}. Since the thermo-optic coefficient of silicon dioxide is much smaller that that of silicon ($\partial n_{SiO2}/\partial T \approx 10^{-5}1/K$ [27]), the temperature dependence of n_{clad} can be safely ignored. Additionally, due to the small influence of n_{clad} on the temperature, the thermo-optic coefficient of the effective refractive index, n_{eff}, can be approximated to be the same as that of silicon ($\partial n_{eff}/\partial T \approx \partial n_{Si}/\partial T$).

Also, the distance d_{Ant} between neighboring antennas as well as the period Λ of the grating change due to thermal expansion. However, since the thermal expansion coefficient $CTE_{Si} = 2.6 \cdot 10^{-6}1/K$ [28] is much smaller than its thermo-optic coefficient, this dependence can also be neglected.

Finally, the emission wavelength λ of semiconductor lasers also depends on the temperature. However, since in most cases laser sources are separated from the photonic IC [29], and their temperature is individually stabilized, this dependency is not considered here. Nevertheless, it must be noted that in systems such as [23], [24], in which laser sources are integrated within the photonic IC, the influence of temperature on the emission wavelength must be also considered.

Due to the temperature dependence of the different variables defining the steering angles ψ and ϑ, it becomes evident that thermal distortions lead to errors in both angles. The errors can be quantified by calculating the angular offsets $\Delta\psi = \psi_{real} - \psi_{desired}$ and $\Delta\vartheta = \vartheta_{real} - \vartheta_{desired}$.

In the following, analytical expressions describing the relation between the angular offsets $\Delta\psi$ and $\Delta\vartheta$ and both types of thermal distortions are presented. The influence of temperature offsets ΔT_{offset} and of temperature gradients ∇T are considered independently. Furthermore, since defining temperature gradients (in K/mm) requires specific dimensions of the OPAs, to generalize the investigations, the expressions provided here use temperature differences (in Kelvin) between individual channels of the OPA.

2.2 Distortions on the Wavelength Controlled Angle

Temperature offsets changing the refractive index of silicon and hence the effective refractive index n_{eff} of the grating antennas, lead to offsets in the wavelength controlled steering angle ψ. Ignoring the influence of thermal expansion on the grating period Λ and the laser temperature to be stabilized independently from the OPA, the effective refractive index n_{eff} shows the largest temperature dependence. Furthermore, considering thermal distortions leading to small angular errors ($\sin(\psi) \approx \psi$), the angular offset $\Delta\psi$ is expected to be:

$$\Delta\psi = \frac{\partial n_{eff}/\partial T}{n_{clad}} \cdot (T - T_{ref}) \tag{6}$$

A detailed derivation of Equation (6) can be found in Appendix A.

While the relation between temperature offsets $\Delta T_{offset} = T - T_{ref}$ and the angular position ψ can be directly recognized, additional discussion is required to understand the relation between these angles and temperature gradients. To determine the influence of temperature gradients, the grating antennas are virtually separated in N sections of equal length, each of which has a different temperature T. The change of the refractive index due to the different temperatures in the individual sections is calculated and the average refractive index $\overline{n}$ over all sections is used to determine the steering angle ψ. It is found that the average refractive index resulting due to presence of temperature gradients can be estimated as the refractive index change due to a temperature rise equal to the average temperature difference over the complete antenna $\overline{T}$ (i.e. $\overline{n} = n(\overline{T})$). A mathematical demonstration of this can be found in Appendix B.

It must be noted that to determine the influence of temperature gradients on the OPA response, the orientation of the temperature gradients relative to the grating antennas should also be considered. However, due to the small dimension of the grating antennas along the x-direction, only temperature gradients parallel to the grating antennas need to be considered here. In case that temperature gradients perpendicular to the antenna array are present, their influence can also be estimated by calculating the average refractive index change of the antennas. Therefore, regardless

of the orientation, the influence of temperature gradients on the wavelength controlled steering angle can be estimated using Equation (6), in the same way as the influence of temperature offsets.

2.3 Distortions on the Phase Controlled Angle

According to Equation (1), the angle ϑ is defined by the relative phase difference between neighboring channels of the array. Furthermore, as described in Equation (5), temperature variations lead to changes in the total accumulated phase $\Delta\varphi$. Therefore, thermal distortions responsible for changes in the relative phase difference between neighboring channels lead to offsets in the steering angle ϑ.

Similar as in the previous section, the influence of thermal expansion, and of the temperature dependence of the laser emission wavelength are ignored, so that the only temperature dependent variable in Equation (1) is the relative phase difference $\Delta\varphi$. Replacing Equation (5) into Equation (1) the relation between the steering angle ϑ and the temperature is found:

$$\sin(\vartheta) = \frac{L}{d_{\text{Ant}}} \cdot \frac{\partial n}{\partial T} \cdot (T - T_{\text{ref}}) \tag{7}$$

where L stands for the length of the waveguide, modulator or antenna, through which light travels.

Temperature offsets ΔT_{offset}, if homogeneous within the complete optical phased array, lead to homogeneous refractive index changes in every channel of the array. This constant refractive index change leads to an equal change of the accumulated phase shift $\Delta\varphi$ in all channels, so that the relative phase difference $\Delta\varphi$ between neighboring channels remains the same. Since ϑ depends on the relative phase difference between neighboring channels, no influence on the angle ϑ is to be expected.

Once again determining the influence of temperature gradients on the steering angle ϑ, the orientation of the temperature gradients relative to the components of the optical phased array must be considered. Similarly as before, to determine the influence of gradients parallel to the channels of the phased array, the optical components are virtually divided in N sections of equal length and it is assumed that each section is at a homogeneous temperature T. The total accumulated phase shift of a single channel of the OPA, due to the presence of parallel temperature gradients, can then be determined by the average temperature $\overline{T}$ along that channel. The relation between the real phase shift and the desired phase shift (i.e. phase shift in absence of temperature gradients) is given by:

$$\Delta\varphi_{\text{real}} = \frac{\overline{T}}{T_{\text{ref}}} \cdot \Delta\varphi_{\text{desired}} \tag{8}$$

Therefore, temperature gradients perfectly parallel to the light propagation direction of the optical phased array, influence the accumulated phase in the same way as a temperature offset equals to the average temperature $\overline{T}$. Therefore, no influence of parallel temperature gradients on the steering angle ϑ is expected. A detailed derivation of Equation (8) can be found in Appendix C.

On the contrary, temperature gradients perpendicular to the light propagation direction (i.e. perpendicular to the individual channels of the optical phased array) lead to different temperatures in each channel of the array. The different temperatures in the single channels lead to different refractive indices and hence to different phase differences between the neighboring channels. Therefore, a temperature difference $\Delta T_{\text{difference}}$ between neighboring channels of the OPA would lead to an additional phase shift and hence to an angular offset $\Delta\vartheta$. Considering small angular errors and replacing the temperature difference $\Delta T_{\text{difference}}$ between neighboring channels into $T - T_{\text{ref}}$ in Equation (7), the angular offset $\Delta\vartheta$ is found to be:

$$\Delta\vartheta \approx \frac{L}{d_{\text{Ant}}} \cdot \frac{\partial n}{\partial T} \cdot \Delta T_{\text{difference}} \tag{9}$$

A detailed deviation of Equation (9) can be found in Appendix D.

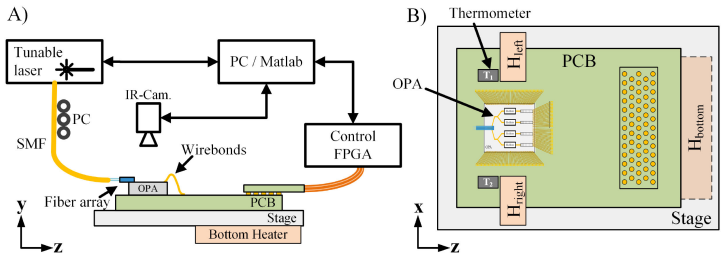

Fig. 2. A) Schematic representation of the measuring setup (side-view). B) Top view of the measuring setup showing the position of the used heaters and thermometers.

3. Experimental Methods

To validate the analytical expressions provided in Section 2, a silicon photonic optical phased array fabricated as part of a multi-project wafer run was characterized using the setup shown in Figure 2. As shown in Figure 2A, light from a tunable laser source is coupled through a grating coupler using an array of single mode optical fibers, glued on top of the photonic IC. The phase of the individual channels of the OPA is controlled using optical modulators, which are driven using an FPGA. The FPGA and the laser source are controlled using Matlab. Light emitted from the OPA is collected through a Fourier microscope by an infrared camera. Each camera pixel corresponds to 0.0299 $^\circ$/pixel.

To analyze the influence of thermal distortions on the steering angles of the OPA, these distortions are intentionally induced using silicone heaters. As shown in Figure 2B, one heater (H_{bottom}) is placed below the system to create temperature offsets. Two additional heaters (H_{left} and H_{right} in Figure 2B) are placed on top of the PCB, on the sides of the OPA to create temperature gradients perpendicular to the light propagation direction (z-direction). The temperature is measured using k-type thermometers (T_1 and T_2) on top of the PCB at the position where the heaters are placed.

Furthermore, a thermal camera was used to determine the relation between the temperature measured at the PCB (i.e. T_{PCB}) and the temperature of the OPA chip (T_{OPA}). It was found that when using the bottom heater, after the system temperature stabilizes, the OPA and the PCB temperature are the same. Since temperature differences in the PCB $\Delta T_{PCB} = T_1 - T_2$ lead to much smaller temperature differences in the OPA ΔT_{OPA}, it is particularly important to determine the relation between both. It was found that in the used setup over the temperature range of interest, the relation between ΔT_{PCB} and ΔT_{OPA} is given by: $\Delta T_{OPA} \approx (5\%) \cdot \Delta T_{PCB}$.

To allow the temperature to stabilize, the optical emission of the OPA was recorded every 10 seconds. Finally, to avoid influence of calibration on the measurement results, the measurements are repeated using different calibrations each time.

4. Experimental Validation of Analytical Expressions

In this section, the results of the optical characterization of the silicon photonic OPA are presented and compared to the analytical models provided in Section 2.

4.1 Measured Influence of Temperature Offsets

In order to determine the influence of temperature offsets on the beam steering angles, the OPA system was heated up. It is expected that heat generated by the silicon heater spreads through the metallic stage and the PCB leading to homogeneous temperature offsets on the OPA.

The results obtained from the optical measurements are presented in Figure 3. Figure 3A shows the angular offsets $\Delta\vartheta$ and $\Delta\psi$ as well as the measured temperature offset over the measuring time. To obtain the relation between the angular offset and the temperature offset, the temperature and the measured angles are averaged over the time period where the temperature has stabilized. In Figure 3, the averaged angular offsets over the averaged temperature are plotted. The measured

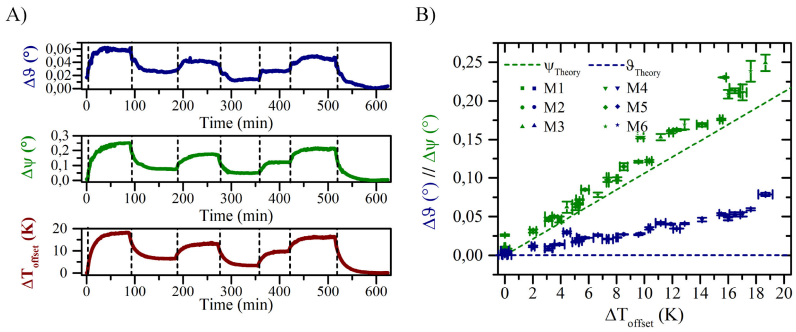

Fig. 3. Influence of temperature offsets on the steering angles ϑ and ψ. A) Comparison of the angular offsets and temperature offset over time for an individual calibration. B) Overview of the angular offset $\Delta\vartheta$ and $\Delta\psi$ caused due to the temperature offsets ΔT_{offset}.

TABLE 1

Comparison of the Expected and Experimentally Determined Behavior of the Beam Steering Angles ϑ and ψ in Case of Temperature Offsets. The Temperature Offset ΔT_{offset} Refers to the Difference Between the Temperature Measured on the PCB to the Room Temperature

Model	$\Delta\vartheta_{\text{model}} = 0$		$\Delta\psi_{\text{model}} = \frac{\partial n_{\text{eff}}/\partial T}{n_{\text{clad}}} \cdot \Delta T_{\text{offset}}$	
	$\Delta\vartheta_{\text{fit}} = m \cdot \Delta T_{\text{offset}} + c$		$\Delta\psi_{\text{fit}} = m \cdot \Delta T_{\text{offset}} + c$	
	m in °/K	c in °	m in °/K	c in °
Theory	0.0	0.0	0.011	0.0
Experiment	(0.003 ± 0.000)	(0.000 ± 0.000)	(0.013 ± 0.000)	(0.007 ± 0.003)

values are fitted and the results from the linear fit are compared to the analytical models presented in Section 2. The results of these fits are shown in Table 1.

Table 1 shows a comparison between the theoretically expected and the experimentally determined behavior of the angular offsets of both steering angles. It must be noted that due to the fact that the temperature is measured on the PCB rather than in the OPA, small deviations might occur. It can be clearly seen, that the wavelength controlled angle ψ agrees reasonably well with theory. On the other hand, the phase controlled steering angle shows an unexpected linear relation between the angular offset $\Delta\vartheta$ and the temperature offset. Since the deflection angle ϑ depends only on the relative phase difference $\Delta\varphi$, as explained in Section 2, homogeneous temperature offsets ΔT_{offset} should not influence the phase controlled emission angle ϑ of the optical phased array. The reason for this unexpected behavior is attributed to an uneven distribution of the adhesive with which the OPA is glued on the PCB, leading to a slightly inhomogeneous temperature distribution on the OPA.

4.2 Measured Influence of Perpendicular Temperature Gradients

To determine the influence of temperature gradients on the beam steering angles, the heaters H_{left} and H_{right} placed on top of the PCB are used to intentionally generate temperature gradients in the system. As discussed in Section 2, the influence of temperature gradients on the beam steering angles depend on the orientation of these gradients relative to the light propagation direction. Since gradients parallel to the light propagation direction act as temperature offsets, here only the effect of gradients perpendicular to the light propagation direction is investigated. Furthermore, since perpendicular temperature gradients influence both angles differently, in the following the influence of temperature gradients on the both angles is individually investigated.

Influence on Phase Controlled Angle ϑ: According to Equation (9), the presence of temperature gradients in the system leads to angular offsets proportional to the temperature difference between neighboring antennas. Due to the small distance between neighboring antennas, rather than using the temperature difference between antennas, the temperature difference across the

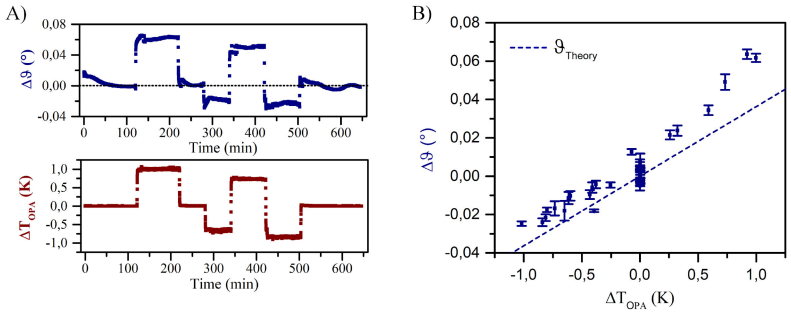

Fig. 4. Influence of temperature gradients on the steering angle ϑ. A) Comparison of the temperature difference across the OPA chip ΔT_{OPA} to the angular offset $\Delta\vartheta$ for an individual calibration. B) Overview of the angular offset $\Delta\vartheta$ caused due to temperature gradients.

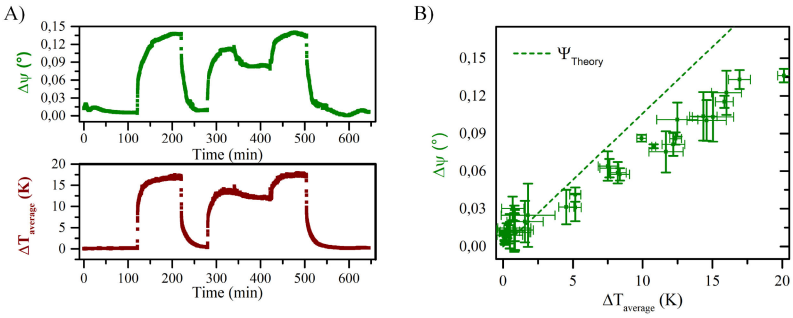

Fig. 5. Influence of temperature gradients on the steering angle ψ. A) Comparison of the average temperature rise to the angular offset $\Delta\psi$ for an individual calibration. B) Overview of the angular offset $\Delta\psi$ caused due to temperature gradients.

OPA chip ΔT_{OPA} is used. As explained in Section 3, the temperature difference across the OPA is estimated to be equal to 5% of the measured temperature difference on the PCB ($\Delta T_{\text{OPA}} \approx 0.05 \cdot \Delta T_{\text{PCB}}$). ΔT_{PCB} is determined as the difference between the temperature measured by the independent thermometers (i.e. $\Delta T_{\text{PCB}} = T_1 - T_2$).

In Figure 4, the results obtained for the phase controlled steering angle are presented. Figure 4A, shows the comparison between the measured temperature difference and the measured angular offset $\Delta\vartheta$. It can be clearly seen, that the angular offset follows well the temperature difference. Even abrupt temperature changes lead to abrupt changes in the steering angle.

Similar as for temperature offsets, the measured angles are averaged over the period of time where the temperature has stabilized and the averaged angles are plotted over the measured temperature difference. Figure 4B, shows the linear fit of the angular offset $\Delta\vartheta$ over the measured temperature difference ΔT_{PCB} for several measurements with different calibrations. The dashed line in Figure 4B, shows the relation described by the analytical equations. It can be seen that the measurements are in reasonable agreement with the theoretical expectation.

Influence on Wavelength Controlled Angle ψ: As discussed in Section 2, in first order approximation, the influence of perpendicular temperature gradients on the wavelength controlled steering angle ψ is described by the refractive index change due to a temperature offset equal to the average temperature (i.e. $\Delta n = n(\overline{T}) - n(T_{\text{reference}})$). Therefore, to estimate the refractive index change Δn, the measured temperatures T_1 and T_2 are averaged to obtain $\overline{T}$.

Figure 5A shows the measured angular offset $\Delta\psi$ as well as the averaged measured temperature $\overline{T}$. It can be easily recognized that $\Delta\psi$ follows well the average temperature offset $\Delta T_{\text{average}} = \overline{T} - T_{\text{reference}}$. As in the previous cases, the averaged angular offsets $\Delta\psi$ for several measurements with different calibrations are plotted vs. the average temperature rise $\Delta T_{\text{average}}$ and a linear fit is performed over the measured values. In Figure 5B, it can be seen that the measured values

TABLE 2

Comparison of Theoretically Expected and Experimentally Determined Behavior of the Steering Angles ϑ and ψ in Case of Temperature Gradients. For the Angle ϑ, the Temperature Difference ΔT_{OPA} is Obtained From the Measured Temperature Difference ΔT_{PCB}. For the Angle ψ, the Averaged Measured Temperature Rise $\Delta T_{\text{average}}$ is Used as the Temperature Offset ΔT_{offset} of the System

Model	$\Delta\vartheta_{\text{model}} = \frac{L}{d_{\text{Ant}}} \cdot \frac{\partial n}{\partial T} \cdot \Delta T_{\text{difference}}$		$\Delta\psi_{\text{model}} = \frac{\partial n_{\text{eff}}/\partial T}{n_{\text{clad}}} \cdot \Delta T_{\text{offset}}$	
	$\Delta\vartheta_{\text{fit}} = m \cdot \Delta T_{\text{OPA}} + c$		$\Delta\psi_{\text{fit}} = m \cdot \Delta T_{\text{average}} + c$	
	m in °/K	c in °	m in °/K	c in °
Theory	0.036	0.0	0.011	0.0
Experiment	(0.038 ± 0.003)	(0.005 ± 0.002)	(0.007 ± 0.000)	(0.007 ± 0.001)

match reasonably well with the theoretical expectations. The reason for the larger deviations in the determined angular offsets $\Delta\psi$ (compare error bars in Figure 5B to those in Figure 3B) might be related to the fact that while perpendicular temperature gradients lead to a different change of the refractive index of each antenna, so that each antenna would emit light to a slightly different angle ψ, the measured angle is the superposition of the different angles at which the antennas emission occurs.

The comparison between the theoretical expectations and the results from the linear fits from Figures 4B as well as from Figure 5B are shown in Table 2. Note that replacing the temperature offset $\Delta T_{\text{offset}} = T - T_{\text{ref}}$ in Equation (6) by the average temperature rise $\Delta T_{\text{average}}$ allows to describe offsets $\Delta\psi$ due to perpendicular gradients in the same way as described for temperature offsets.

5. Conclusions

In this contribution, the influence of thermal distortions on the steering angles ϑ and ψ of silicon photonic optical phased arrays has been investigated. Analytical expressions describing the influence of temperature offsets and gradients on both angles have been derived and experimentally validated.

While the provided expressions describe reasonably well the thermal response of the OPA, there are still deviations between the theoretically expected response and the experimentally measured response. One possible explanation for these deviations is the fact that the provided expressions consider ideal rather than real OPAs.[1] A further explanation might be that the phase shifting efficiency of the modulators also depends on the temperature, so that the temperature dependent behavior of the optical modulators should also be taken into account.

While it has been demonstrated that thermal distortions have a significant impact on the steering angles of the optical phased array, if detected, they can be compensated either by re-calibration, by compensation of temperature gradients or by modification of the emission wavelength of the laser source. The demonstration of the compensation of temperature gradients is out of the scope of this work and will be presented in a following contribution.

Despite the fact that additional investigations are required to fully understand the thermal behavior of OPAs, it is possible to conclude, that precise understanding as well as proper compensation of the thermal distortions pave the way for silicon photonic optical phased arrays replacing mechanical systems to become the next generation beam steering systems.

Appendix A
Detailed Derivation of Equation (6)

In this Appendix, a detailed deviation of Equation (6) is presented. Equation (6), relates the wavelength controlled steering angle ψ to temperature offsets $\Delta T_{\text{offset}} = T - T_{\text{ref}}$. Temperature

[1] The main difference between ideal and real OPAs is that due to imperfections during the fabrication (i.e. due to fabrication tolerances) there are small discrepancies in the geometry of the channels length and width, leading to different n_{eff} and hence to different accumulated phases. This is the same reason, why real OPA systems must be calibrated prior their use.

offsets lead to changes in the refractive index and hence deviations in the emission angle ψ. Therefore, the relation between temperature and the steering angle ψ can be found by considering the temperature dependence of the refractive index. Equation (10) defines the dependence of the steering angle ψ on the temperature T.

$$\sin(\psi) = \frac{n_{\text{eff}} + \frac{\partial n_{\text{eff}}}{\partial T} \cdot (T - T_{\text{ref}}) - \frac{\lambda}{\Lambda}}{n_{\text{clad}} \cdot + \frac{\partial n_{\text{clad}}}{\partial T} \cdot (T - T_{\text{ref}})} \approx \frac{n_{\text{eff}} - \frac{\lambda}{\Lambda}}{n_{\text{clad}}} + \frac{\partial n_{\text{eff}}/\partial T}{n_{\text{clad}}} \cdot (T - T_{\text{ref}}) \tag{10}$$

Assuming the thermo-optic coefficient of the cladding to be much smaller than that of silicon, the angular offset $\Delta\psi$ is found to be:

$$\psi(T) = \psi_{\text{real}} = \frac{n_{\text{eff}}(T_0) - \frac{\lambda}{\Lambda}}{n_{\text{clad}}} + \frac{\partial n_{\text{eff}}/\partial T}{n_{\text{clad}}} \cdot (T - T_0) = \psi_{\text{desired}} + \psi_{\text{error}} \tag{11}$$

Rearranging Equation (11) and assuming $\Delta\psi = \psi_{\text{real}} - \psi_{\text{desired}}$ Equation (6) is found.

Appendix B
Influence of Temperature Gradients on Refractive Index

To estimate the influence of temperature gradients on the beam steering angles of an optical phased array, in Section 2 it was assumed that the refractive index n of the components in the OPA can be estimated as the refractive index change due to a temperature offset equal to the average temperature $\overline{T}$. This hypothesis is demonstrated in this section.

Hypothesis: The average refractive index change, Δn, due to the presence of temperature gradients along an optical component, is equal to the refractive index change due to a homogeneous temperature offset equal to the average temperature $\overline{T}$ of the component.

To prove that hypothesis, it is shown that the average refractive index $\overline{n}$ of an optical component in the presence of temperature gradients equals the refractive index of that component at the average temperature (i.e. $\overline{n} = n(\overline{T})$). Therefore, the proof consists of two steps: first, the optical component is virtually divided in N sections of equal length, the average temperature $\overline{T}$ of the component is determined and the refractive index at $T = \overline{T}$ is calculated. Then, the refractive index of the N sections of the components is averaged $\overline{n}$ and the result is compared to $n(\overline{T})$.

Step 1: Divide component into N sections of equal length and assume that each section j of the component is at a homogeneous temperature T_j. Assuming linear temperature gradients, the temperature T_j of each section is given by:

$$T_j = T_1 + (j-1) \cdot \Delta T \tag{12}$$

Using Equation (12), the average temperature, $\overline{T} = \frac{1}{N}\sum_{j=1}^{N} T_j$ is found to be:

$$\overline{T} = \frac{1}{N}\sum_{j=1}^{N} T_1 + \frac{1}{N}\sum_{j=1}^{N}(j-1) \cdot \Delta T = T_1 + \frac{\Delta T}{N}\sum_{j=1}^{N}(j-1) \tag{13}$$

Using the arithmetic sum identity $\sum_{j=1}^{N}(j-1) = \frac{N(N-1)}{2}$, Equation (13) is simplified to:

$$\overline{T} = T_1 + \frac{\Delta T}{2} \cdot (N-1) \tag{14}$$

Replacing the temperature T in Equation (3) by the average temperature from Equation (14) and assuming $T_1 = T_{\text{ref}}$, the refractive index at the average temperature is found to be:

$$n\left(\overline{T}\right) = n(T_1) + \frac{\partial n}{\partial T} \cdot \left(\overline{T} - T_1\right) = n(T_1) + \frac{\partial n}{\partial T} \cdot \left(\frac{\Delta T}{2} \cdot (N-1)\right) \tag{15}$$

Step 2: The next step is to average the refractive index of the N sections of the component.

$$\overline{n} = \frac{1}{N}\sum_{j=1}^{N} n(T_j) = \frac{1}{N}\sum_{j=1}^{N} n(T_1) + \frac{1}{N}\sum_{j=1}^{N} \frac{\partial n}{\partial T}\cdot(T_j - T_1) = n(T_1) + \frac{1}{N}\sum_{j=1}^{N} \frac{\partial n}{\partial T}\cdot(T_j - T_1) \tag{16}$$

Replacing Equation (12) into Equation (16) the average refractive index is found to be:

$$\overline{n} = n(T_1) + \frac{\Delta T}{N}\cdot\frac{\partial n}{\partial T}\cdot\sum_{j=1}^{N}(j-1) = n(T_1) + \frac{\partial n}{\partial T}\cdot\left(\frac{\Delta T}{2}\cdot(N-1)\right) = n(T_1) + \frac{\partial n}{\partial T}\cdot\left(\overline{T} - T_1\right) = n(\overline{T}) \tag{17}$$

Since the result presented in Equation (17) is identical to the one from Equation (15), it is possible to conclude that $\overline{n} = n(\overline{T})$ and hence that the influence of temperature gradients on the refractive index is in first order approximation the same as that of a homogeneous temperature offset equal to the average temperature $\overline{T}$.

Appendix C
Influence of Parallel Temperature Gradients on Accumulated Phase Shift

The accumulated phase difference due to changes in the refractive index along a waveguide of length L is defined as: $\Delta\varphi = \int_0^L \frac{2\pi}{\lambda}\cdot\Delta n(z)\mathrm{d}z$. Considering temperature gradients parallel to the light propagation direction, the accumulated phase shift becomes:

$$\Delta\varphi = \frac{2\pi}{\lambda}\cdot\frac{\partial n}{\partial T}\cdot\int_0^L \Delta T(z)\mathrm{d}z \tag{18}$$

Dividing the optical component in N sections of equal length, the phase after each segment k is given by:

$$\varphi_k = \varphi_{k-1} + \frac{2\pi}{\lambda}\cdot\frac{\partial n}{\partial T}\cdot L\cdot T_1 = \varphi_0 + \frac{2\pi}{\lambda}\cdot\frac{\partial n}{\partial T}\cdot L\cdot\sum_{j=1}^{k} T_j \tag{19}$$

For $k = N$ the phase difference $\Delta\varphi_{\text{real}}$ between the the start and the end of the waveguide is given by:

$$\Delta\varphi_{\text{real}} = \varphi_N - \varphi_0 = \frac{2\pi}{\lambda}\cdot\frac{\partial n}{\partial T}\cdot L\cdot(T_1 + T_2 + \cdots + T_N) = \frac{2\pi}{\lambda}\cdot\frac{\partial n}{\partial T}\cdot L\cdot\sum_{j=1}^{N} T_j \tag{20}$$

Assuming linear gradients, replacing T_j from Equation (12) and using the sum identity $\sum_{j=1}^{N} c = c\cdot N$ and the Arithmetic series:

$$\Delta\varphi_{\text{real}} = \frac{2\pi}{\lambda}\cdot\frac{\partial n}{\partial T}\cdot L\cdot N\cdot T_1 + \frac{2\pi}{\lambda}\cdot\frac{\partial n}{\partial T}\cdot L\cdot N\cdot\frac{\Delta T}{2}\cdot(N-1) \tag{21}$$

Considering there would be no temperature gradient along the waveguide, the accumulated phase $\Delta\varphi_{\text{desired}}$ would be given by:

$$\Delta\varphi_{\text{desired}} = \frac{2\pi}{\lambda}\cdot\frac{\partial n}{\partial T}\cdot L_{\text{total}}\cdot T_1 \tag{22}$$

where the total length of the waveguide is given by: $L_{\text{total}} = N\cdot L$. Rearranging Equation (21):

$$\Delta\varphi_{\text{real}} = \Delta\varphi_{\text{desired}} + \frac{\Delta\varphi_{\text{desired}}}{T_1}\cdot\frac{\Delta T}{2}\cdot(N-1) = \Delta\varphi_{\text{desired}}\cdot\left(1 + \frac{1}{T_1}\cdot\frac{\Delta T}{2}\cdot(N-1)\right) \tag{23}$$

In Equation (14) the average temperature of the component was found to be: $\overline{T} = T_1 + \frac{\Delta T}{2} \cdot (N-1)$. Replacing that average temperature in Equation above:

$$\Delta\varphi_{\text{real}} = \Delta\varphi_{\text{desired}} \cdot \left(1 + \frac{\overline{T} - T_1}{T_1}\right) = \Delta\varphi_{\text{desired}} \cdot \frac{\overline{T}}{T_1} \tag{24}$$

Appendix D
Detailed Derivation of Equation (9)

In this Appendix, a detailed deviation of Equation (9) is presented. Equation (9), relates the phase controlled steering angle ϑ to temperature differences between neighboring channels of the optical phased array. Temperature gradients perpendicular to the light propagation direction within the optical phased array lead to different temperatures and hence different refractive index in each channel of the array. From Equation (4) it is known that the accumulated phase difference is directly related to the refractive index change along a waveguide. Considering the thermally induced phase shift from Equation (5) to be an error adding to the desired phase shift $\Delta\varphi_{\text{desired}}$, the real phase shift in each channel is found to be:

$$\Delta\varphi_{\text{real}} = \Delta\varphi_{\text{desired}} + \Delta\varphi_{\text{error}} = \Delta\varphi_{\text{desired}} + \frac{2\pi}{\lambda} \cdot L \cdot \frac{\partial n}{\partial T} \cdot \Delta T \tag{25}$$

Replacing Equation (25) into Equation (1) and assuming gradients leading to small angular errors:

$$\vartheta_{\text{real}} \approx \frac{\lambda}{2\pi \cdot d_{\text{Ant}}} \cdot \Delta\varphi_{\text{desired}} + \frac{L}{d_{\text{Ant}}} \cdot \frac{\partial n}{\partial T} \cdot \Delta T = \vartheta_{\text{desired}} + \vartheta_{\text{error}} \tag{26}$$

Rearranging Equation (26) and assuming $\Delta\vartheta = \vartheta_{\text{real}} - \vartheta_{\text{desired}}$, Equation (9) is found.

References

[1] H. Guo, X. Wang, J. Li, and J. Shang, "Research review on the development of liquid crystal optical phased array device on the application of free space laser communication," *Proc. SPIE*, vol. 10841, Jan. 2019, Art. no. 108410C. [Online]. Available: https://www.spiedigitallibrary.org/conference-proceedings-of-spie/10841/2509434/Research-review-on-the-development-of-liquid-crystal-optical-phased/10.1117/12.2509434.full

[2] H.-W. Rhee, M. Kim, J.-B. You, and H.-H. Park, "High-Speed data transmission with beam-steering using silicon optical phased array," in *Proc. 21st Int. Conf. Adv. Commun. Technol.*, Feb. 2019, pp. 212–216. [Online]. Available: https://ieeexplore.ieee.org/document/8701956/

[3] C. V. Poulton *et al.*, "Long-Range LiDAR and free-space data communication with high-performance optical phased arrays," *IEEE J. Sel. Topics Quantum Electron.*, vol. 25, no. 5, pp. 1–8, Sep. 2019. [Online]. Available: https://ieeexplore.ieee.org/document/8678389/

[4] A. Tuantranont, V. Bright, J. Zhang, W. Zhang, J. Neff, and Y. Lee, "Optical beam steering using MEMS-controllable microlens array," *Sensors Actuators A, Phys.*, vol. 91, no. 3, pp. 363–372, Jul. 2001. [Online]. Available: http://linkinghub.elsevier.com/retrieve/pii/S0924424701006094

[5] J. Kim *et al.*, "1100 x 1100 port MEMS-based optical crossconnect with 4-dB maximum loss," *IEEE Photon. Technol. Lett.*, vol. 15, no. 11, pp. 1537–1539, Nov. 2003. [Online]. Available: http://ieeexplore.ieee.org/document/1237580/

[6] F. Filhol, E. Defaÿ, C. Divoux, C. Zinck, and M.-T. Delaye, "Resonant micro-mirror excited by a thin-film piezoelectric actuator for fast optical beam scanning," *Sensors Actuators A, Phys.*, vol. 123/124, pp. 483–489, Sep. 2005. [Online]. Available: https://linkinghub.elsevier.com/retrieve/pii/S0924424705003328

[7] P. Brandl, S. Schidl, A. Polzer, W. Gaberl, and H. Zimmermann, "Optical wireless communication with adaptive focus and MEMS-based beam steering," *IEEE Photon. Technol. Lett.*, vol. 25, no. 15, pp. 1428–1431, Aug. 2013. [Online]. Available: http://ieeexplore.ieee.org/document/6525314/

[8] J. Sun, E. Timurdogan, A. Yaacobi, E. S. Hosseini, and M. R. Watts, "Large-scale nanophotonic phased array," *Nature*, vol. 493, no. 7431, pp. 195–199, Jan. 2013. [Online]. Available: http://www.nature.com/doifinder/10.1038/nature11727

[9] J. Kim, M. N. Miskiewicz, S. Serati, and M. J. Escuti, "Nonmechanical laser beam steering based on polymer polarization gratings: Design optimization and demonstration," *J. Lightw. Technol.*, vol. 33, no. 10, pp. 2068–2077, May 2015. [Online]. Available: http://ieeexplore.ieee.org/document/7009951/

[10] J. K. Doylend, M. J. R. Heck, J. T. Bovington, J. D. Peters, L. A. Coldren, and J. E. Bowers, "Two-dimensional free-space beam steering with an optical phased array on silicon-on-insulator," *Opt. Express*, vol. 19, no. 22, Oct. 2011, Art. no. 21595. [Online]. Available: https://www.osapublishing.org/oe/abstract.cfm?uri=oe-19-22-21595

[11] N. A. Tyler *et al.*, "SiN integrated optical phased arrays for two-dimensional beam steering at a single near-infrared wavelength," *Opt. Express*, vol. 27, no. 4, Feb. 2019, Art. no. 5851. [Online]. Available: https://www.osapublishing.org/abstract.cfm?URI=oe-27-4-5851
[12] P. F. Wang *et al.*, "Improving the performance of optical antenna for optical phased arrays through high-contrast grating structure on SOI substrate," *Opt. Express*, vol. 27, no. 3, Feb. 2019, Art. no. 2703. [Online]. Available: https://www.osapublishing.org/abstract.cfm?URI=oe-27-3-2703
[13] T. Komljenovic, R. Helkey, L. Coldren, and J. E. Bowers, "Sparse aperiodic arrays for optical beam forming and LIDAR," *Opt. Express*, vol. 25, no. 3, Feb. 2017, Art. no. 2511. [Online]. Available: https://www.osapublishing.org/abstract.cfm?URI=oe-25-3-2511
[14] M. R. Kossey, C. Rizk, and A. C. Foster, "End-fire silicon optical phased array with half-wavelength spacing," *APL Photon.*, vol. 3, no. 1, Jan. 2018, Art. no. 011301. [Online]. Available: http://aip.scitation.org/doi/10.1063/1.5000741
[15] P. McManamon *et al.*, "Optical phased array technology," *Proc. IEEE*, vol. 84, no. 2, pp. 268–298, Feb. 1996. [Online]. Available: http://ieeexplore.ieee.org/document/482231/
[16] S.-C. Wooh and Y. Shi, "Influence of phased array element size on beam steering behavior," *Ultrasonics*, vol. 36, no. 6, pp. 737–749, Apr. 1998. [Online]. Available: https://linkinghub.elsevier.com/retrieve/pii/S0041624X97001649
[17] Y. Jin, J. Wu, A. Yan, Z. Hu, Z. Zhao, and W. Shi, "Optimum beam steering of optical phased arrays using mixed weighting technique," *Optik*, vol. 125, no. 16, pp. 4568–4571, Aug. 2014. [Online]. Available: https://linkinghub.elsevier.com/retrieve/pii/S0030402614003544
[18] G. N. Malheiros-Silveira, L. H. Gabrielli, C. J. Chang-Hasnain, and H. E. Hernandez-Figueroa, "Breakthroughs in photonics 2013: Advances in nanoantennas," *IEEE Photon. J.*, vol. 6, no. 2, pp. 1–6, Apr. 2014. [Online]. Available: http://ieeexplore.ieee.org/document/6766176/
[19] B. J. Frey, D. B. Leviton, and T. J. Madison, "Temperature-dependent refractive index of silicon and germanium," *Proc. SPIE*, vol. 6273, Jun. 2006, Art. no. 62732J. [Online]. Available: http://proceedings.spiedigitallibrary.org/proceeding.aspx?doi=10.1117/12.672850
[20] S. Chung, H. Abediasl, and H. Hashemi, "A monolithically integrated large-scale optical phased array in silicon-on-insulator CMOS," *IEEE J. Solid-State Circuits*, vol. 53, no. 1, pp. 275–296, Jan. 2018. [Online]. Available: http://ieeexplore.ieee.org/document/8071147/
[21] L. Zhang, X. Sun, W. Zhang, G. Wang, N. Feng, and W. Zhao, "Compact optical phased array using a serial grating antenna design," 2019. [Online]. Available: https://arxiv.org/abs/1903.04573
[22] S. Zhu *et al.*, "CMOS-compatible integrated silicon nitride optical phase array for electrically tunable off-chip laser beam steering," in *Proc. Electron. Devices Technol. Manuf. Conf.*, Mar. 2019, pp. 228–230. [Online]. Available: https://ieeexplore.ieee.org/document/8731179/
[23] W. Guo *et al.*, "Two-Dimensional optical beam steering with InP-Based photonic integrated circuits," *IEEE J. Sel. Topics Quantum Electron.*, vol. 19, no. 4, Jul. 2013, Art. no. 6100212. [Online]. Available: http://ieeexplore.ieee.org/document/6407678/
[24] J. C. Hulme *et al.*, "Fully integrated hybrid silicon two dimensional beam scanner," *Opt. Express*, vol. 23, no. 5, Mar. 2015, Art. no. 5861. [Online]. Available: https://www.osapublishing.org/abstract.cfm?URI=oe-23-5-5861
[25] H. Abediasl and H. Hashemi, "Monolithic optical phased-array transceiver in a standard SOI CMOS process," *Opt. Express*, vol. 23, no. 5, Mar. 2015, Art. no. 6509. [Online]. Available: https://www.osapublishing.org/abstract.cfm?URI=oe-23-5-6509
[26] S. Chung, H. Abediasl, and H. Hashemi, "15.4 A 1024-element scalable optical phased array in 0.18 μm SOI CMOS," in *Proc. IEEE Int. Solid-State Circuits Conf.*, Feb. 2017, pp. 262–263. [Online]. Available: http://ieeexplore.ieee.org/document/7870361/
[27] D. B. Leviton and B. J. Frey, "Temperature-dependent absolute refractive index measurements of synthetic fused silica," *Proc. SPIE*, vol. 6273, Jun. 2006, Art. no. 62732K. [Online]. Available: http://proceedings.spiedigitallibrary.org/proceeding.aspx?doi=10.1117/12.672853
[28] J. R. Rumble, D. R. Lide, and T. J. Bruno, *CRC Handbook of Chemistry and Physics: A Ready-Reference Book of Chemical and Physical Data*, 99th ed. Boca Raton, FL, USA: CRC Press, 2018.
[29] G. Pan *et al.*, "Ultra-compact electrically controlled beam steering chip based on coherently coupled VCSEL array directly integrated with optical phased array," *Opt. Express*, vol. 27, no. 10, May 2019, Art. no. 13910. [Online]. Available: https://www.osapublishing.org/abstract.cfm?URI=oe-27-10-13910